

Tunable entanglement generation for mobile–electron spin qubits

A. I. Signal

Institute of Fundamental Sciences, Massey University, Private Bag 11 222, Palmerston North, New Zealand

U. Zülicke*

*Institute of Fundamental Sciences and MacDiarmid Institute for Advanced Materials and Nanotechnology,
Massey University, Private Bag 11 222, Palmerston North, New Zealand*

(Dated: November 23, 2018)

Recent studies have shown that linear electron optics can be used to generate entangled two–particle states from nonentangled ones if additional measurements of charge or parity are performed. We have investigated such nondeterministic entanglement production in electronic versions of the Mach–Zehnder interferometer, where spin–dependent interference occurs due to the presence of electric–field tuneable Rashba spin splitting. Adjustment of the spin–precession length turns out to switch the entangler on and off, as well as control the detailed form of entangled output states.

Entanglement is seen as an important resource for quantum information processing (QIP), enabling exponential speed-up of classically hard computations, secure cryptography, and ultradense coding of information.¹ Generating entanglement in the electronic spin degree of freedom is therefore essential for many solid–state–based QIP schemes.² Several proposals rely on two–particle correlation effects induced, e.g., by superconducting leads,³ Coulomb blockade in quantum dots,⁴ or quasiparticle collisions.⁵ It is, however, possible to obtain spin–entangled two–electron states in the absence of interactions using scattering interference at beam splitters.^{6,7,8} This opens up a promising avenue for realizing QIP based on linear fermion optics⁸ as a solid–state analog of efficient quantum computation with photons.⁹

Our present study combines recent insight into linear–optics QIP with the possibilities of spin–dependent electron interference.^{10,11} We find that maximally entangled mobile electron pairs can be extracted at the output of an electronic Mach–Zehnder (MZ) interferometer, realized in an asymmetric semiconductor heterostructure, using a projective charge measurement. The efficiency of entanglement generation depends on the spin–precession length L_{so} for electrons in the interferometer arms and is therefore tuneable by external gate voltages. The same is true for the detailed form of entangled two–qubit states that are generated. Hence it is possible to accomplish electric–field control of entanglement production and entangled–state output in the device considered here.

The basic setup and transport properties of a spin–dependent electronic MZ interferometer were studied theoretically in Ref. 11. (See Ref. 12 for a recent experimental realization of a MZ interferometer *without* spin dependence.) It is a four–terminal (two–input, two–output) device where electron–wave interference depends on spin due to the presence of Rashba spin splitting.¹³ Linear conductances were calculated based on a spin–resolved single–electron scattering matrix for the entire interferometer. For our present study, we investigated *two–electron* interference in this system, which is a nontrivial generalization because the Pauli principle affects the outcome of multi–particle scattering events.¹⁴ Two–particle interference at beam splitters can be used for detecting entanglement,¹⁵ and spin precession from Rashba spin splitting offers a way to manipulate entangled states.¹⁶ We proceed

now to briefly sketch our theoretical description.

The two–particle Hilbert space for electrons at any four–terminal device is six–dimensional. We find it useful to use a magic basis of Bell states¹⁷

$$|\chi_1\rangle = \frac{1}{\sqrt{2}} \left(c_{a+}^\dagger c_{a-}^\dagger + c_{b+}^\dagger c_{b-}^\dagger \right) |0\rangle, \quad (1a)$$

$$|\chi_2\rangle = \frac{1}{\sqrt{2}} \left(c_{a+}^\dagger c_{b+}^\dagger - c_{a-}^\dagger c_{b-}^\dagger \right) |0\rangle, \quad (1b)$$

$$|\chi_3\rangle = \frac{1}{\sqrt{2}} \left(c_{a+}^\dagger c_{b-}^\dagger + c_{a-}^\dagger c_{b+}^\dagger \right) |0\rangle, \quad (1c)$$

$$|\chi_4\rangle = \frac{i}{\sqrt{2}} \left(c_{a+}^\dagger c_{a-}^\dagger - c_{b+}^\dagger c_{b-}^\dagger \right) |0\rangle, \quad (1d)$$

$$|\chi_5\rangle = \frac{i}{\sqrt{2}} \left(c_{a+}^\dagger c_{b+}^\dagger + c_{a-}^\dagger c_{b-}^\dagger \right) |0\rangle, \quad (1e)$$

$$|\chi_6\rangle = \frac{i}{\sqrt{2}} \left(c_{a+}^\dagger c_{b-}^\dagger - c_{a-}^\dagger c_{b+}^\dagger \right) |0\rangle, \quad (1f)$$

where the operator $c_{\alpha\sigma}^\dagger$ creates an electron at the Fermi energy in the interferometer arm α and with Rashba spin–subband quantum number σ . Any two–electron state $|i\rangle$ ($|o\rangle$) at the input (output) can be expressed as a linear combination of these basis states. It is straightforward to derive the 6×6 two–particle scattering matrices S_{2el} that relate two–particle input and output states for each linear–optics element (such as beam splitters, mirrors, and the spin–dependent phases acquired when the electrons propagate through interferometer arms). As examples, we give the one for an ideal symmetric beam splitter,

$$S_{2el}^{(bs)} = \begin{pmatrix} 0 & \frac{1}{\sqrt{2}} & 0 & 0 & 0 & \frac{1}{\sqrt{2}} \\ \frac{1}{\sqrt{2}} & -\frac{1}{2} & 0 & 0 & 0 & \frac{1}{2} \\ 0 & 0 & -1 & 0 & 0 & 0 \\ 0 & 0 & 0 & -1 & 0 & 0 \\ 0 & 0 & 0 & 0 & -1 & 0 \\ -\frac{1}{\sqrt{2}} & -\frac{1}{2} & 0 & 0 & 0 & \frac{1}{2} \end{pmatrix}, \quad (2)$$

and the one describing propagation through inner interferometer arms (horizontal and vertical device dimensions given by x and y , respectively) where the spin–precession length enters:

$$\mathcal{S}_{2\text{el}}^{(\text{Ra})} = \begin{pmatrix} 1 & 0 & 0 & 0 & 0 & 0 & 0 \\ 0 & -\cos\left(\frac{\pi(x+y)}{L_{\text{so}}}\right) & 0 & 0 & 0 & \sin\left(\frac{\pi(x+y)}{L_{\text{so}}}\right) & 0 \\ 0 & 0 & -\cos\left(\frac{\pi(x-y)}{L_{\text{so}}}\right) & 0 & 0 & 0 & \sin\left(\frac{\pi(x-y)}{L_{\text{so}}}\right) \\ 0 & 0 & 0 & -1 & 0 & 0 & 0 \\ 0 & -\sin\left(\frac{\pi(x+y)}{L_{\text{so}}}\right) & 0 & 0 & -\cos\left(\frac{\pi(x+y)}{L_{\text{so}}}\right) & 0 & 0 \\ 0 & 0 & \sin\left(\frac{\pi(x-y)}{L_{\text{so}}}\right) & 0 & 0 & 0 & \cos\left(\frac{\pi(x-y)}{L_{\text{so}}}\right) \end{pmatrix}. \quad (3)$$

Suitable combination of the respective matrices for beam splitters, mirrors, etc. yields the scattering matrix $\mathcal{S}_{2\text{el}}^{(\text{MZI})}$ for the entire MZ interferometer, which depends on the device dimensions measured in units of the spin-precession length. Its analytical form is unilluminating, hence we omit it here. With this result, we can discuss two-electron scattering interference at spin-dependent MZ interferometers in full generality.

We focus on a specific situation where the input is a two-particle product state with double-occupancy in one interferometer arm. See Fig. 1 for an illustration. Without loss of generality, we choose the state $|i_{\text{dbl}}\rangle = c_{a+}^\dagger c_{a-}^\dagger |0\rangle$. In general, the output state generated from it by the MZ interferometer will be a quantum superposition of states having single electron occupancy in each output arm with others that have a finite amplitude for double occupancy in one of them. Let's assume we have the means to measure the electron number (i.e., charge) in one of the output channels (e.g., in arm b). Performing this measurement each time we send in two electrons with opposite spin at the input channel a, we will obtain

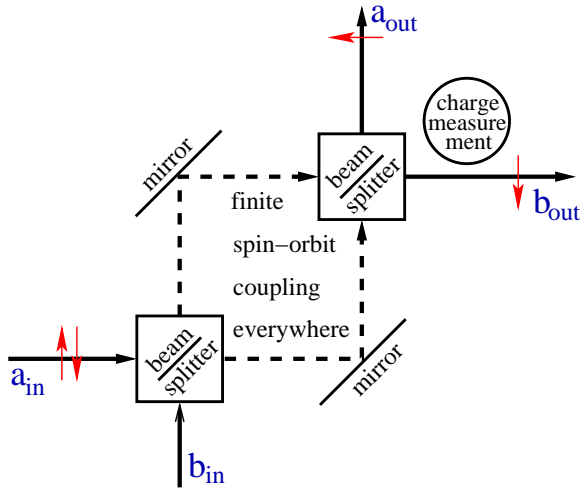


FIG. 1: (Color online) Entanglement generation at a spin-dependent Mach-Zehnder interferometer. A two-particle product state is incident in channel a, as indicated. The output state generated by the interferometer is projected, by a charge measurement, onto its component with single electron occupancy in each output arm. The resulting two-electron state turns out to be maximally entangled in the electrons' quantum number for spin projection perpendicular to their respective interferometer arm, i.e., Rashba spin-subband index.

the values 0, 1, or 2 with certain frequencies. The charge measurement leaves the spin and orbital wave functions of output states unaffected, but it allows us to filter out, e.g., such states where exactly one electron is scattered into each of the output arms. We have calculated the concurrence¹⁸ (i.e., a measure of entanglement) for the single-occupancy output states that are generated from the double-occupancy input state $|i_{\text{dbl}}\rangle$ given above and found that they are *always maximally entangled*, irrespective of interferometer geometry and size. Hence, preparing the input state $c_{a+}^\dagger c_{a-}^\dagger |0\rangle$, which can be achieved by simply raising the voltage in the electron reservoir connected to input a by a certain amount, and choosing states at the interferometer output for which exactly one electron lives in each output arm, we obtain two-electron states that are maximally entangled in the Rashba spin quantum number σ . A schematic illustration of this procedure is shown in Fig. 1. Our analysis shows that the same entangled output state is generated when the two-electron input is incident in interferometer arm b instead. To perform the crucial charge measurement, mesoscopic electrometers such as single-electron transistors or quantum point contacts could be employed.⁸

The efficiency P_{eg} for nondeterministic entanglement generation as described above is obviously given by the probability of single-electron occupancy per output arm for the

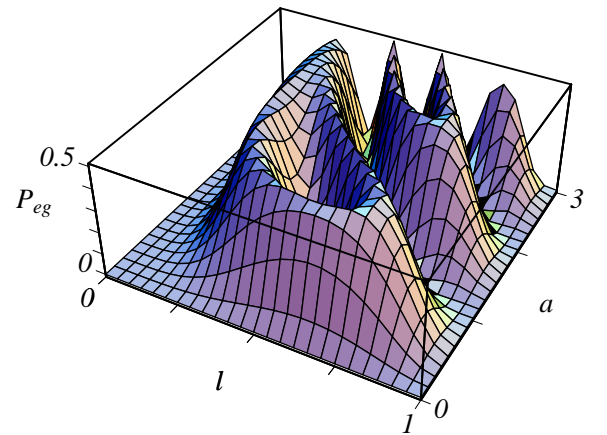


FIG. 2: (Color online) Efficiency P_{eg} of entanglement generation by the procedure illustrated in Fig. 1, calculated for rectangular MZ interferometers of width lL_{so} and aspect ratio a .

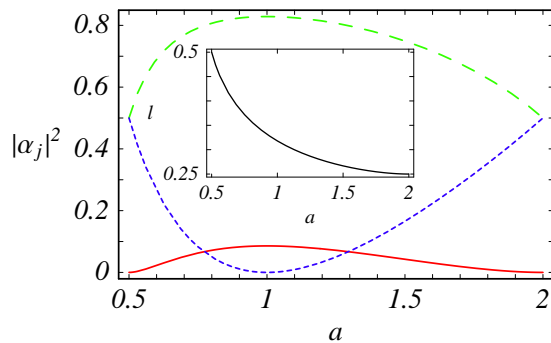


FIG. 3: (Color online) Admixture of Bell basis states in the output state generated for interferometer configurations with maximal efficiency of entanglement generation. The solid curve shows the overlap with χ_2 , which is identical to that with the state χ_6 . The overlap with states χ_3 and χ_5 is given by the short-dashed and long-dashed curves, respectively. Inset: Smallest value of dimensionless interferometer width l for given aspect ratio a at which the maximum entanglement-generation efficiency of 50% is realized.

state $\mathcal{S}_{2\text{el}}^{(\text{MZI})} |i_{\text{dbl}}\rangle$). This quantity depends on the interferometer size and geometry but turns out to be the same for a double-occupancy state incident in channel b. In the following, we consider a rectangularly shaped MZ interferometer of width w and height h , using the dimensionless parameters $l = w/L_{\text{so}}$ and $a = h/w$ for its characterization. We find

$$P_{\text{eg}} = \frac{1}{2} - \frac{1}{8} \left\{ \sin^2([a-1]l\pi) + \sin^2([a+1]l\pi) + \cos(2l\pi) + \cos(2al\pi) \right\}^2. \quad (4)$$

Figure 2 illustrates the existence of maxima in P_{eg} as a function of l for given finite a . As can be seen from Eq. (4), the largest possible value of P_{eg} is 50%, which is the same as the efficiency of entanglement generation at a single beam splitter.⁶ Unlike the beam splitter, however, the MZ interferometer can be tuned by an external gate voltage (which controls the parameter l by adjusting¹⁹ L_{so}) between maxi-

um and zero entanglement generation, realizing a switchable entangler. Further investigation may show possibilities for increasing the entanglement-generation efficiency by cascading several MZ interferometers in series.⁶ Any backscattering incurred from the charge measurement is detrimental for the output of entangled electron pairs and will have to be minimized, e.g., by using a highly sensitive²⁰ and efficient²¹ quantum-point-contact electrometer.

We proceed to examine in greater detail the entangled state generated by the above procedure. Due to the projection, it lives in the subspace spanned by the Bell states χ_2 , χ_3 , χ_5 , and χ_6 . We find for the respective amplitudes

$$\alpha_2 = -\alpha_6 = \sin(2l\pi) \sin(2al\pi) / (4\sqrt{P_{\text{eg}}}) \quad , \quad (5a)$$

$$\alpha_3 = \sin(l\pi) \sin([a-1]l\pi) \sin(al\pi) / \sqrt{P_{\text{eg}}} \quad , \quad (5b)$$

$$\alpha_5 = \sin(l\pi) \sin([a+1]l\pi) \sin(al\pi) / \sqrt{P_{\text{eg}}} \quad . \quad (5c)$$

As external gate voltages can adjust the value of l , it is possible to control the detailed form of entangled output states generated by a given interferometer setup. Situations where the efficiency of entanglement production reaches its maximal value of 50% are of greatest practical interest, hence we investigate those further. As Fig. 2 indicates, there may exist more than one value of dimensionless interferometer width l for which P_{eg} is maximized at a given aspect ratio a . To be specific, we consider always the smallest of such l values in the following, as plotted in the inset of Fig. 3. The overlap of maximum-efficiency output states with Bell basis states is shown in Fig. 3. Bell states that are symmetric under spin reversal generally provide the largest contribution.

In conclusion, we presented a procedure for generating entangled electron pairs using spin-dependent interferometry and a projective charge measurement. Electric-field control of the spin precession length enables manipulation of the entangled output state and realization of a switchable entangler.

We benefitted from useful discussions with M. Governale, J. König, and Y. Tokura. UZ gratefully acknowledges support from the Marsden Fund of the Royal Society of New Zealand.

* Electronic address: u.zuelicke@massey.ac.nz

¹ M. A. Nielsen and I. L. Chuang, *Quantum Computation and Quantum Information* (Cambridge U Press, Cambridge, 2000).

² D. D. Awschalom, N. Samarth, and D. Loss, eds., *Semiconductor Spintronics and Quantum Computation* (Springer, Berlin, 2002).

³ P. Recher, E. V. Sukhorukov, and D. Loss, *Phys. Rev. B* **63**, 165314 (2001); G. B. Lesovik, T. Martin, and G. Blatter, *Eur. Phys. J. B* **24**, 287 (2001); C. Bena, S. Vishveshwara, L. Balents, and M. P. A. Fisher, *Phys. Rev. Lett.* **89**, 037901 (2002).

⁴ W. D. Oliver, F. Yamaguchi, and Y. Yamamoto, *Phys. Rev. Lett.* **88**, 037901 (2002); D. S. Saraga and D. Loss, *ibid.* **90**, 166803 (2003).

⁵ D. S. Saraga, B. L. Altshuler, D. Loss, and R. M. Westervelt, *Phys. Rev. Lett.* **92**, 246803 (2004).

⁶ S. Bose and D. Home, *Phys. Rev. Lett.* **88**, 050401 (2002).

⁷ C. W. J. Beenakker, C. Emary, M. Kindermann, and J. L. van

Velsen, *Phys. Rev. Lett.* **91**, 147901 (2003); P. Samuelsson, E. V. Sukhorukov, and M. Büttiker, *ibid.* **92**, 036805 (2004).

⁸ C. W. J. Beenakker, D. P. DiVincenzo, C. Emary, and M. Kindermann, *Phys. Rev. Lett.* **93**, 020501 (2004).

⁹ E. Knill, R. Laflamme, and G. J. Milburn, *Nature* **409**, 46 (2001).

¹⁰ J. Nitta, F. E. Meijer, and H. Takayanagi, *Appl. Phys. Lett.* **75**, 695 (1999).

¹¹ U. Zülicke, *Appl. Phys. Lett.* **85**, 2616 (2004).

¹² Y. Ji, Y. Chung, D. Sprinzak, M. Heiblum, D. Mahalu, and H. Strikman, *Nature (London)* **422**, 415 (2003).

¹³ Y. A. Bychkov and E. I. Rashba, *J. Phys. C* **17**, 6039 (1984).

¹⁴ R. Loudon, *Phys. Rev. A* **58**, 4904 (1998).

¹⁵ G. Burkard, D. Loss, and E. V. Sukhorukov, *Phys. Rev. B* **61**, R16303 (2000).

¹⁶ J. C. Egues, G. Burkard, and D. Loss, *Phys. Rev. Lett.* **89**, 176401 (2002); *Appl. Phys. Lett.* **82**, 2658 (2003).

- ¹⁷ K. Eckert, J. Schliemann, D. Bruß, and M. Lewenstein, *Ann. Phys. (NY)* **299**, 88 (2002).
- ¹⁸ W. K. Wootters, *Phys. Rev. Lett.* **80**, 2245 (1998).
- ¹⁹ J. Nitta, T. Akazaki, H. Takayanagi, and T. Enoki, *Phys. Rev. Lett.* **78**, 1335 (1997); G. Engels, J. Lange, T. Schäpers, and H. Lüth, *Phys. Rev. B* **55**, R1958 (1997).
- ²⁰ M. Field, C. G. Smith, M. Pepper, D. A. Ritchie, J. E. F. Frost, G. A. C. Jones, and D. G. Hasko, *Phys. Rev. Lett.* **70**, 1311 (1993).
- ²¹ S. Pilgram and M. Büttiker, *Phys. Rev. Lett.* **89**, 200401 (2002).